Clays and Clay Minerals, Vol. 56, No. 5, 511–519, 2008.

SOME PHYSICOCHEMICAL PROPERTIES OF THE WHITE SEPIOLITE KNOWN AS PIPESTONE FROM ESKİŞEHİR, TURKEY

MÜŞERREF ÖNAL*, HAMZA YILMAZ, AND YÜKSEL SARIKAYA

Department of Chemistry, Faculty of Science, Ankara University, Tandoğan, 06100 Ankara, Turkey

Abstract—Various physicochemical characteristics of a sepiolite sample from the Eskişehir area, Turkey, were investigated to help in making predictions about possible uses of the material. The sample was examined by chemical analysis (CA), thermal analysis (DTA/TGA), X-ray diffraction (XRD) analysis, particle-size analysis (PSA), linear dilatometry (LD), scanning electron microscopy (SEM), mercury porosimetry (Hg-Por.), and low-temperature nitrogen adsorption/desorption (N_2-AD) techniques. The CA and XRD data indicated that the sepiolite contains only 6% dolomite by mass. The XRD patterns showed that sepiolite anhydride, enstatite, diopside, and opal-CT form upon heating the sepiolite above 600, 800, 900, and 1200ºC, respectively. The maximum rate of endothermic changes in the DTA and TGA curves were observed at 82, 287, and 491ºC, corresponding to the loss of external, zeolitic, and bound water from the sepiolite, respectively. Dehydroxylation and recrystallization of the sepiolite were fastest at 845ºC and 862ºC, respectively. The LD curve indicated that the shrinkage began at 800ºC and reached 4.0% at 1000ºC. The proportion of particles with diameters of <2 μm, and the external surface area of the long-term (24 h) water-treated sepiolite were determined by PSA as 79% by volume, and 8 m^2g^{-1}, respectively. The SEM view revealed discrete bundles of sepiolite fibers of various lengths. The specific surface area found from adsorption data was 316 m^2g^{-1}. The specific micro-, meso-, macro-, and total-pore volumes obtained from the combination of Hg-Por. and N_2-AD results were 0.16, 0.21, 0.45, and 0.82 cm^3g^{-1}, respectively. The average macropore and micro-mesopore radii in the sepiolite were estimated (using the Hg-Por. and N_2-AD data) to be 35 and 2.4 nm, respectively.

Key Words—Porosity, Sepiolite, Surface Area, Thermal Analysis, X-ray Diffraction.

INTRODUCTION

Sepiolite is a hydrous magnesium silicate clay mineral with a fibrous morphology. Its theoretical half-unit cell formula is given as $Si_{12}O_{30}Mg_8(OH)_4(OH_2)_4.8H_2O$ (Preisinger, 1959; Weir *et al.*, 2002; McKeown *et al.*, 2002). Sepiolite occurrences have been reported in the USA, Kenya, Spain, Portugal, Turkey, Saudi Arabia, Great Britain, Morocco, and elsewhere (Post, 1978; Galán and Ferrero, 1982). Turkish sepiolites are found in Eskişehir and northwest Anatolia (Kadir *et al.*, 2002; Akbulut and Kadir, 2003; Yalçın and Bozkaya, 1995, 2004; Karakaya *et al.*, 2004).

The most important Turkish sepiolite, which is white in color, is mined in Eskişehir and is known as pipestone. It has been mined and used since the early ages of the Roman Empire (Ece and Çoban, 1994). The main early use was in carving sculptures and a significant amount of waste was discarded in the process. Today, the production of tobacco pipes and carved souvenir items also produces some waste, and the sample used in this study was taken from the wastes of such products. The chemical composition, crystal structure, and morphology of the Eskişehir sepiolite have been examined extensively (Otsuka *et al.*, 1973; Yücel *et al.*, 1980; Inukai *et al.*, 1994; Arık *et al.*, 1996). However, few studies have focused on the thermal behavior and porosity of the material (Akıncı, 1967; Balcı, 1996; Özdemir and Kıpçak, 2004; Esmer, 2004). This study reports some physicochemical properties of a sample from Eskişehir sepiolites.

MATERIAL AND METHODS

A sepiolite (pipestone) sample was taken from the Eskişehir region of Turkey. Chemical analysis was carried out on an Hitachi Z-8200 Atomic Absorption Spectrophotometer (Kahraman *et al*., 2005). The results were calculated as the mass percentages of the metal oxides. The cation exchange capacity (CEC) was determined by the methylene blue procedure (Hang and Brindley, 1970; Rywto *et al.*, 1991). Five similar sepiolite samples, taken from other beds in Eskişehir, were also analyzed and their CECs determined.

The natural sepiolite samples (10 g each) were heated at various temperatures, at 100ºC intervals, up to 1300ºC, and were brought to thermal equilibrium by keeping them at each temperature for 2 h. The XRD patterns of the natural and heat-treated samples were obtained from random mounts using a Rikagu D-Max 2200 Powder Diffractometer with CuKα radiation and a Ni filter. The XRD patterns of the five similar sepiolite samples from Eskişehir were then recorded. The DTA

* E-mail address of corresponding author:
onal@science.ankara.edu.tr
DOI: 10.1346/CCMN.2008.0560504

and TGA curves of the sepiolite were recorded on a Shimadzu Apparatus (DTG-60H) at a heating rate of 10ºC min^{-1}, between 25 and 1000ºC. The linear dilatometric curve of a natural sepiolite rod with $30 \times 3 \times 3$ mm dimensions were obtained using a Netzsch STA 429 instrument in the temperature range 25−1000ºC.

The volumetric particle-size distribution (PSD) and external specific surface area (S_{ext}) of the sepiolite sample that was kept in water for 24 h were determined using a Mastersizer Instrument (Malvern, Micron Model). In this experiment, the suspension, which was prepared using an arbitrary amount of sepiolite powder, was added dropwise to distilled water in the cell. The morphology of the sepiolite was examined by SEM, using a JEOL JSM-490LV instrument operating at an accelerating voltage of 15 kV. For comparison, the SEM images of the five similar sepiolite samples from Eskişehir were also recorded.

The macro-mesopore size distribution of the natural sepiolite was determined by a mercury intrusion porosimeter (Micromeritics, Model 910). The sample was dried in an oven at 105ºC for 48 h prior to testing. Triply distilled mercury was used in the experiment. The adsorption/desorption of N_2 on the sepiolite at 77 K was investigated by a volumetric adsorption instrument of Pyrex glass connected to high vacuum of 10^{-5} mm of Hg (Sarıkaya and Aybar, 1978; Sarıkaya *et al.*, 2000). Before adsorption, the sample was outgassed at 150ºC for 4 h under a vacuum of 10^{-5} mm Hg. The first relative equilibrium pressure for the first data point was taken as zero.

RESULTS AND DISCUSSION

Chemical analysis

The CA of the natural sepiolite (in mass %) was: SiO_2, 55.45; MgO, 26.53; Al_2O_3, 0.85; Fe_2O_3, 0.07; TiO_2, 0.06; CaO, 1.86; Na_2O, 0.06; K_2O, 0.08; and loss on ignition (LOI), 14.60. The CaO may be due to contaminating dolomite ($MgCO_3.CaCO_3$), a non-clay mineral. The MgO derives from both sepiolite and dolomite. The LOI is due to the dehydration and dehydroxylation of the sepiolite, and also the calcination of dolomite. The remainder of the constituents occur naturally as part of the sepiolite. The Al_2O_3, Fe_2O_3, and TiO_2 originate from the isomorphous replacements of Al^{3+}, $Fe^{2+,3+}$, and $Ti^{3+,4+}$ cations with Mg^{2+} in the octahedral and Si^{4+} cations in the tetrahedral chains of the sepiolite (Corma and Peréz-Pariente, 1987). The presence of trivalent cations in octahedral and tetrahedral positions creates some excess positive and negative charges, respectively, which partly compensate each other. Other excess negative charge, if present, is balanced by exchangeable cations. The CEC of this sepiolite was found, by the methylene blue method, to be 0.27 meq g^{-1}.

These results were compared with those from 11 other sepiolite samples from various beds in Eskişehir, five of which were analyzed by the present authors and the remainder by other authors (Akıncı, 1967; Otsuka *et al.*, 1973; Rautureau and Yücel, 1976; Çetişli and Gedikbay, 1990; Sugiura *et al.*, 1991). The results differ slightly depending on the locality of the samples. The variability intervals reported by these different analyses of 12 samples are (mass %): SiO_2, 52−63; MgO, 22−28; Al_2O_3, 0.1−4.0; Fe_2O_3, 0.02−1.50; TiO_2, 0.01−0.30; CaO, 0.15−2.50; Na_2O, 0.02−0.10; K_2O, 0.01−0.30; and LOI, 10−20. Clearly, the metal oxide percentages for the samples examined are between these limits. In addition, the analyses of four different Vallecas sepiolites and two Nevada sepiolites agree approximately with these results (Komarneni *et al.*, 1986; Campelo *et al.*, 1987; Post, 1978). The relative changes in the Al_2O_3, Fe_2O_3, and CaO contents are, consequently, greater than the other components. The CEC interval for 12 different samples from Eskişehir was found to be 10−40 meq g^{-1}. The CEC of the examined sample is between these limits.

XRD and thermal analyses

The XRD pattern of the natural sepiolite (Figure 1) contains two sharp reflections at 1.220 and 0.289 nm,

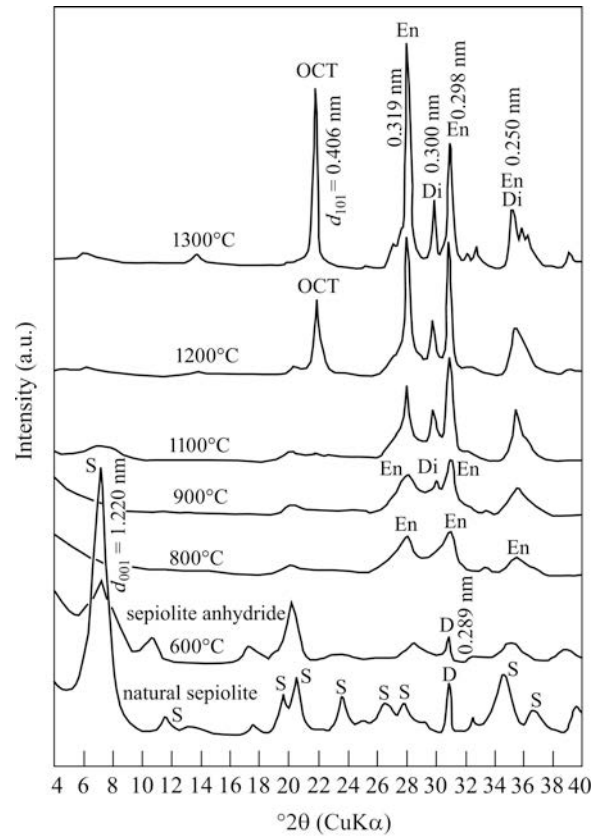

Figure 1. XRD patterns of the natural and heat-treated sepiolite samples (S: sepiolite, D: dolomite, En: enstatite, Di: diopside, OCT: opal-CT)

https://doi.org/10.1346/CCMN.2008.0560504 Published online by Cambridge University Press

which are the most characteristic peaks of sepiolite (S) and dolomite (D), respectively (Moore and Reynolds, 1997). On the basis of the XRD peak intensities, the amount of dolomite appears to be small compared to sepiolite, a result supported by the CA. The percentage of dolomite was calculated stoichiometrically as 5.7% using the CaO content obtained from the CA. Therefore, the mass % of sepiolite must be 94.3%. The SiO_2 and MgO contents of the sepiolite (free of dolomite) were calculated as 52.29% and 25.02%, respectively. The estimated molar ratio of SiO_2:MgO was 2.8:2.0, which is near the theoretical value of 3.0:2.0 based on the chemical formula of sepiolite.

The XRD patterns (not shown) of five other samples of this sepiolite taken from different beds in Eskişehir (not given here) were examined and were similar, but some differences in intensity and width of the most characteristic d_{001} peaks for sepiolite were seen. As a result, chemical and XRD analyses showed that the CEC and crystallinity in the samples changed depending on their localities. Earlier CA and XRD analyses of this sepiolite and other sepiolites obtained similar results (Otsuka *et al.*, 1973; Serna *et al.*, 1975; Kıyohiro and Otsuka, 1989; Ece and Çoban, 1994; Yalçın and Bozkaya, 2004). The most common impurities in sepiolites are dolomite, magnesite, and calcite, according to other XRD data for sepiolites.

The DTA and TGA curves of the sepiolite (Figure 2) are similar to those reported for different samples of the same sepiolite and other sepiolites, but they were not evaluated quantitatively (Akıncı, 1967; Serna *et al.*, 1975; Rautureau and Yücel, 1976; Grillet *et al.*, 1988; Balcı, 1996; Yalçın and Bozkaya, 2004). These DTA and TGA curves were, nevertheless, used to establish temperature intervals and to understand the mechanism for dehydration and dehydroxylation through interpretation of endothermic changes (Otsuka *et al.*, 1973; Kıyohiro and Otsuka, 1989).

With the CA and DTA/TGA data and XRD patterns of the heat-treated samples (Figure 1) in hand, the characteristics of the sepiolite may be described as follows. Six endothermic changes and one exothermic change are seen in the DTA curves. The temperature interval and maximum rate of change are indicated on the DTA and TGA curves (Figure 2). The first major endothermic mass loss of 7.5%, between 25 and 131ºC, with the maximum rate of change of 82ºC, is due to the evolution of interparticle water (W), *i.e.* adsorbed, and some zeolitic water (ZW_1). The second endothermic mass loss of 4.5%, between 131 and 338ºC, with the maximum rate of change of 287ºC, is due to the dehydration of the rest of the zeolitic water (ZW_2). The total of the two mass losses ($W+ZW_1+ZW_2$) at temperatures up to 338ºC is 12.0%. Distinguishing between the dehydration temperatures for the interparticle water and the zeolitic water is not possible.

The third endothermic mass loss of 5.2%, between 338 and 563ºC, with the maximum rate of change at 491ºC, is due to the dehydration of the bound water (BW). Bound water molecules are lost in two steps and these steps are accompanied by a reversible structure change (Serna and Ahlrichs, 1975; Kıyohiro and Otsuka, 1989; Weir *et al.*, 2002). The loss of about half of the bound water by the first dehydration step probably

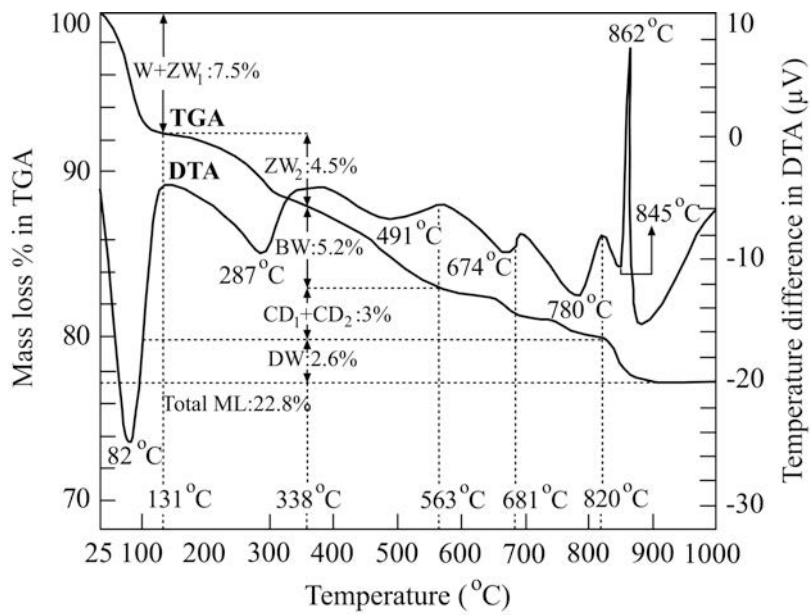

Figure 2. TGA and DTA curves for the natural sepiolite in the temperature range 25–1000ºC. Mass losses are identified as follows: W: adsorbed water; ZW_1: some of the zeolitic water; ZW_2: the remainder of the zeolitic water; BW: bound water; $CD_1 + CD_2$: calcination of dolomite in two steps; and DW: dehydroxylation water.

https://doi.org/10.1346/CCMN.2008.0560504 Published online by Cambridge University Press

causes a partial folding in the nanochannels. Due to the obstruction by these folded channels of the diffusion of the remaining bound water molecules, a decrease in water evolution rate results and consequently total exclusion of water lags behind. The mass-loss percentage due to the bound water must, in any case, be less than or equal to the theoretical value of 5.56%. As the chemical formula suggests, twice as much zeolitic water as bound water is present, and the mass percentage of the zeolitic water in the sepiolite of the natural rock must be 10.4%. The mass percentage of the interparticle water is, therefore, 1.6%. Furthermore, the ratio of the bound-water content, obtained from the TGA curve, to the bound-water content calculated theoretically from the ideal chemical formula of sepiolite, gives (approximately) the mass percent of sepiolite in the natural rock of 94%. The rest is taken as dolomite, i.e. 6%. This result is also supported by the result obtained on the basis of CA. The phase that remains after the dehydration of bound water is called sepiolite anhydride and it has the chemical formula $Si_{12}O_{30}Mg_8(OH)_4$. The d_{001} XRD peak of the sepiolite anhydride decreases in intensity while maintaining its position as the temperature increases (Figure 1).

The fourth endothermic mass loss of 1.5%, between 563ºC and 681ºC, with a maximum rate of change at 674ºC, originates from the first-step calcination of dolomite (CD_1) mainly due to the reaction $MgCO_3{\cdot}CaCO_3 \rightarrow MgO + CO_2 + CaCO_3$.

The fifth mass loss of 1.5%, between 681 and 820ºC, with a maximum rate of change at 780ºC, stems from the second-step calcination (CD_2) by the reaction $CaCO_3 \rightarrow CaO + CO_2$.

The total mass lost through the calcination of dolomite is 3.0%. The mass percentage of dolomite calculated on the basis of CO_2 evolved is 6.3%. The result is consistent with the other results obtained above. The characteristic dolomite peak disappears after heating up to 800ºC (Figure 2).

The sixth endothermic mass loss of 2.6% after 820ºC, with a maximum rate of change at 845ºC, is due to the dehydroxylation of the sepiolite. After the irreversible dehydroxylation, the sepiolite anhydride is transformed to enstatite and then to amorphous silica at 862ºC without any mass loss (Kulbicki, 1959). The reaction can be represented as $Si_{12}O_{30}Mg_8(OH)_4 \rightarrow 4Mg_2Si_2O_6 + 4SiO_2 + 2H_2O$.

The XRD patterns reveal that the enstatite (En) formation begins after heating above 800ºC (Figure 1). Furthermore, diopside forms above 900ºC according to the reaction $CaO + MgO + 2SiO_2 \rightarrow CaMgSi_2O_6$.

The XRD peaks for enstatite intensifies greatly between 800 and 1300ºC as enstatite becomes more crystalline. As the amount of CaO is insufficient to form more diopside, the XRD peaks for the diopside do not increase in intensity. The XRD reflection at 0.406 nm, arising after heating above 1200ºC, represents the formation of a paracrystalline opal-CT (OCT) from the remaining silica (Elzea *et al.*, 1994; Aras, 2004; Kahraman *et al.*, 2005; Önal *et al.*, 2007).

Linear shrinkage

The linear dilatometric (LD) curve of the natural sepiolite (Figure 3) reveals that no striking elongation or shrinkage was observed between 25 and 800ºC. Between 800 and 1000ºC, a linear shrinkage of 4.0% occurred due to the dehydroxylation of sepiolite and calcination of dolomite. The linear shrinkage increased to 5.5% by cooling from 1000 to 200ºC and then decreased to 3.0% until 25ºC depending on the contraction and water adsorption of the calcined sepiolite, respectively. Evidently this is the first report of thermal shrinkage behavior of this material.

Particle-size analysis

The particle-size distribution of the sepiolite, held in aqueous suspension for 24 h, as volumetric percentage *vs.* particle diameter (Vol.% *vs. D*) and its derivative [d(Vol.%)/d*D vs. D*] indicate that the Vol.% of the particles having D of <2 μm was 79% (Figure 4). The mean particle size of the sepiolite was estimated to be 0.5 μm corresponding to the maximum of the derivative curve. Based on a laser-scattering technique for PSD measurements, the external specific surface area (S_{ext}) of the sepiolite particles was determined to be 8 m^2g^{-1}. The S_{ext} is the area of the unit mass solid, having taken the geometrical surface of particles into account but not the area of wall inside the pores.

Morphology

The SEM image of the sepiolite (Figure 5) shows that the texture of the sepiolite agrees well with some previous images (Ece and Çoban, 1994; Yalçın and Bozkaya, 2004). All pores of the natural sepiolite are apparently filled with water. The occurrence of the

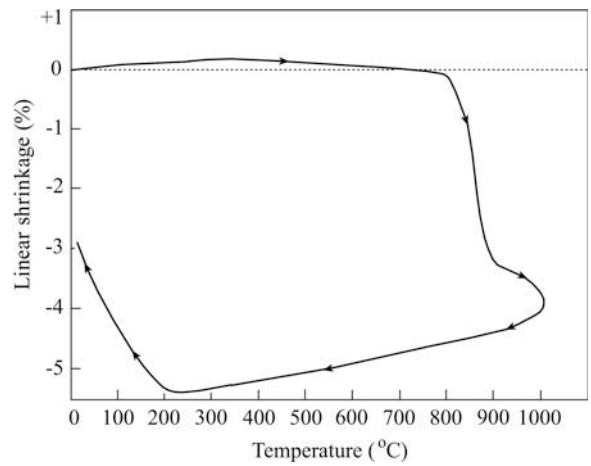

Figure 3. Linear shrinkage curve of the natural sepiolite in the temperature range 25−1000ºC.

https://doi.org/10.1346/CCMN.2008.0560504 Published online by Cambridge University Press

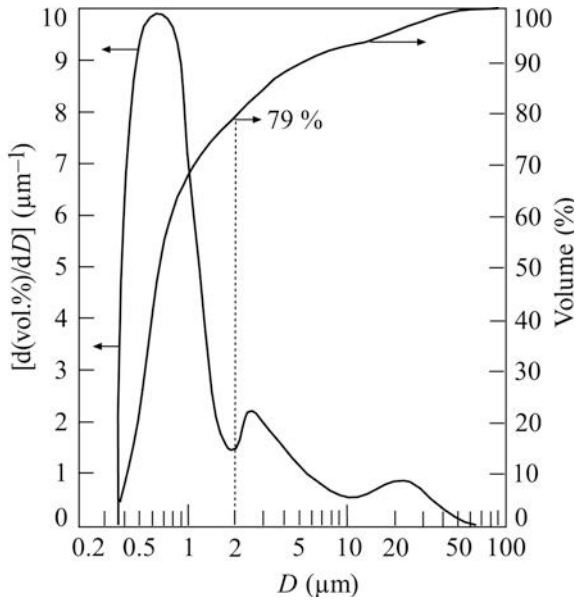

Figure 4. Volumetric particle-size distribution curve as Vol.% *vs. D* and [dVol.%/d*D*] *vs*. *D* of the sepiolite samples held in aqueous suspension for 24 h.

discrete and bundled sepiolite fibers of various lengths is noticeable in the image. Branching of the sepiolite fibers gives rise to a porous morphology. The pores may be of different sizes and cylindrical, parallel-sided slit, wedge, cavity, or ink-bottle shaped. The radius of a pore assumed to be cylindrical can be taken as half of its width. The pores with radii of <1 nm, between 1 and 25 nm, and >25 nm are classified as micro-, meso-, and macropores, respectively. Recently, the pores with radii between 1 and 100 nm were referred to as nanopores (Lu and Zhao, 2004).

Macro- and mesoporosity

Mercury porosimetric pore-size distribution curves in the form of *V vs. r* (Figure 6) were obtained in reverse

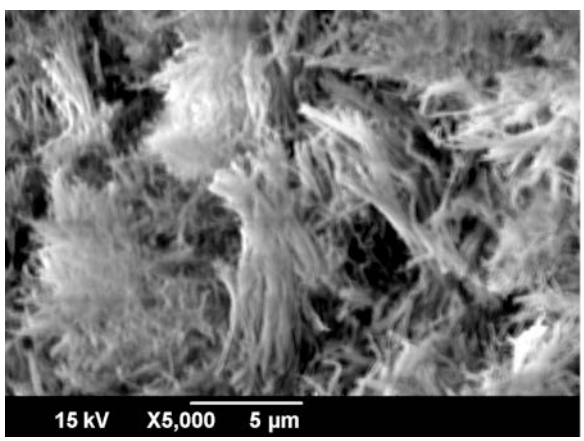

Figure 5. SEM image of the natural sepiolite.

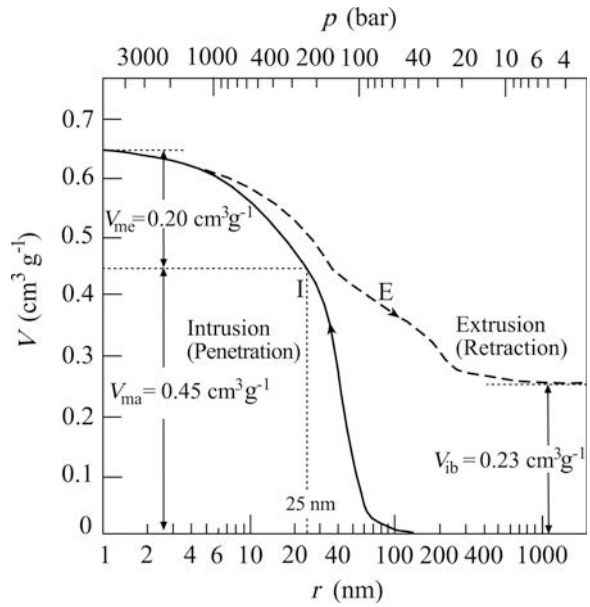

Figure 6. The *V vs. r* pore-size distribution curves for the natural sepiolite obtained from mercury porosimetry by the intrusion (I) and extrusion (E) steps of mercury (*p*: applied pressure, *r*: pore radius, *V*: specific meso–macropore volume, V_{me}: specific mesopore volume, V_{ma}: specific macropore volume, V_{ib}: specific volume of ink-bottle pores).

directions during the intrusion (I) and extrusion (E) of mercury (Fisher and Gaupp, 2004). The difference between the *V vs. r* curves obtained from intrusion and extrusion data is referred to as volume hysteresis (Moscou and Lub, 1981; Kloubek, 1981). Volume hysteresis is due to the pores consisting of large cavities being connected to each other through smaller pores that serve as narrow necks forming voids similar to ink bottles. Since the filling begins from the largest cavities and the expulsion from the narrowest necks, volume hysterisis results. Even after pressure has been reduced to atmospheric pressure, 0.23 cm^3 of mercury remains trapped in 1 g of sepiolite. This shows that the specific volume of the ink-bottle pores is V_{ib} = 0.23 cm^3g^{-1}. The specific macropore volume (V_{ma}) and mesopore volume (V_{me}) of the sepiolite were estimated from the intrusion curve as 0.45 cm^3g^{-1} and 0.20 cm^3g^{-1}, respectively (Figure 6).

The mean macropore radius is read as 35 nm at the maximum of the d*V*/d*r vs. r* curve obtained from intrusion (Figure 7). The radius derivative curve obtained from the extrusion step has two maxima (Figure 7). The mean radius of the narrow and large necks of the ink-bottle pores are read approximately as 35 nm and 150 nm at these maxima. No other report has appeared in the literature on the macropore-size distribution of sepiolite samples with which to compare these findings.

Nitrogen adsorption/desorption isotherms

The N_2 adsorption/desorption isotherms on sepiolite at 77 K were obtained (Figure 8). Here, *n* is the

https://doi.org/10.1346/CCMN.2008.0560504 Published online by Cambridge University Press

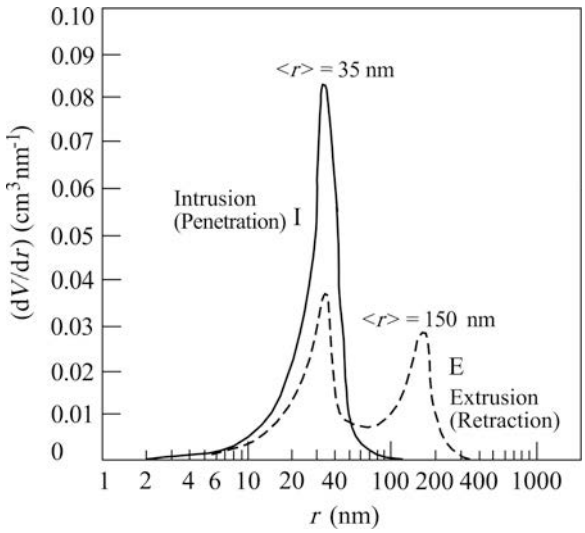

Figure 7. The (dV/dr) *vs.* r pore-size distribution curves for the natural sepiolite by intrusion (I) and extrusion (E) steps of mercury (<r>: average pore radius).

adsorption capacity defined as molar quantity of N_2 on 1 g of solid and $x = p/p^o$ is the ratio of the equilibrium pressure to vapor pressure of liquid nitrogen at the working temperature. The shape of the isotherms indicates that the sepiolite contains micropores along with mesopores and macropores. Hysteresis over the interval $0.80<x<0.96$ is due to the fact that capillary condensation begins at the narrowest mesopores and capillary evaporation at the largest mesopores.

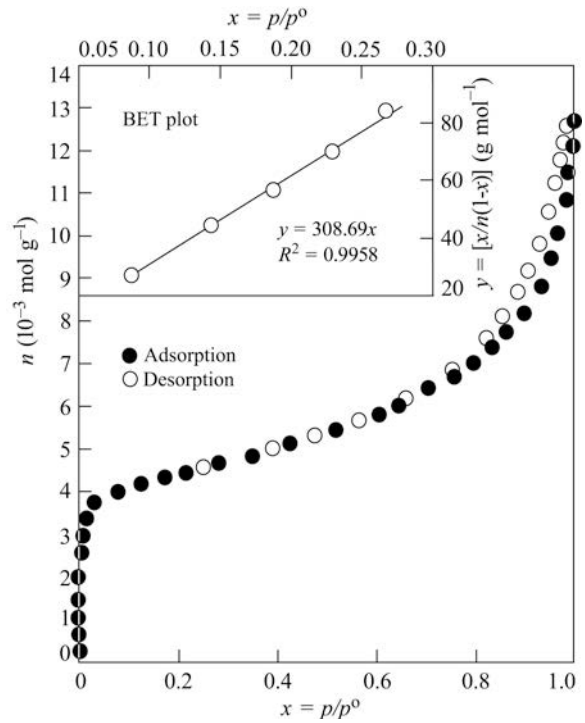

Figure 8. The N_2 adsorption/desorption isotherms at 77 K on the natural sepiolite and the corresponding BET plot (p: adsorption and desorption equilibrium pressure; p^o: vapor pressure of liquid N_2 at the experiment temperature, $p/p_o = x$ relative equilibrium pressure, n: adsorption capacity).

Surface area

Specific surface area (S) is the area of unit mass of the solid, including the area of pores, but not the surface of the intracrystalline channels present in materials such as sepiolite and related minerals. This quantity was obtained by applying the standard Brunauer, Emmett, and Teller (BET) method on the adsorption data relating to the interval $0.05<x<0.35$ (Brunauer *et al.*, 1938; Everett *et al.*, 1974). The S value for the sepiolite is calculated to be 316 m^2g^{-1}, from the slope of the BET straight line (Figure 8). The contribution of the area of the walls of the macrospores, to total surface area, is also negligible. The S values for samples of the same origin and of other origins are between 250 and 360 m^2g^{-1}, depending on their impurities, isomorphous cation exchange, and crystallinity (Grillet *et al.*, 1988; Sugiura *et al.*, 1991; Balcı, 1996).

Micro- and mesoporosity

By using N_2 adsorption data, the specific micropore volume (V_{mi}) was found (using Dubinin's 1967 method) to be 0.16 cm^3g^{-1} (Figure 9). The adsorption capacity as liquid nitrogen volume calculated from desorption data was taken as the specific micro-mesopore volume (V_{mm}) for completely full pores at any x. The molar volume of liquid N_2 was taken as 34.65 cm^3g^{-1}. The radius (r) of

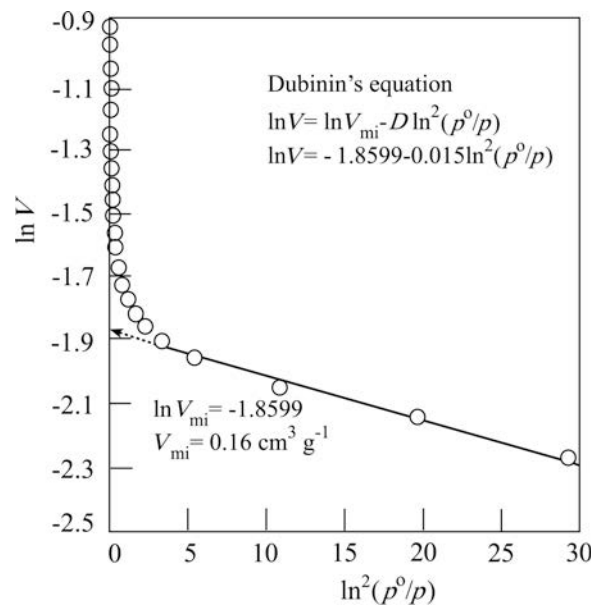

Figure 9. Determination of the specific micropore volume (V_{mi}) of the sepiolite by Dubinin's method.

https://doi.org/10.1346/CCMN.2008.0560504 Published online by Cambridge University Press

the largest filled pore at the same value of x, corresponding to the V_{mm} value, was calculated from the corrected Kelvin equation (Rouquerol *et al.*, 1999). The mesopore size-distribution curves (V_{mm} *vs.* r) and its radius derivative (dV_{mm}/dr *vs.* r) for the sepiolite were also determined (Figure 10).

The V_{mm} and V_{mi} for the sepiolite were estimated from the extrapolated intercepts of the V_{mm} *vs.* r curve to be r = 25 nm and r = 1 nm, respectively, (Figure 10). The V_{mm} and V_{mi} values were 0.37 and 0.16 cm^3g^{-1}, respectively. The V_{mi} values calculated were found to be the same using this method and the Dubinin method. This V_{mi} value does not include the volume of the intracrystalline channels present in sepiolite. The V_{me} was calculated to be $V_{me} = V_{mm} - V_{mi} = 0.37 - 0.16 = 0.21$ cm^3g^{-1}. The V_{me} value agrees well with the value of 0.20 cm^3g^{-1} obtained from mercury porosimetry. The total specific pore volume (V_t) of the sepiolite was calculated by combining the mercury porosimetry and nitrogen adsorption results, *i.e.* $V_t = V_{ma} + V_{me} + V_{mi} = 0.45 + 0.21 + 0.16 = 0.82$ cm^3g^{-1}.

The dV/dr *vs.* r curve spans the interval 1–25 nm, but the peak is at ~2 nm. The average radius of micro-mesopores was calculated as follows:

$$\langle r \rangle = 2 \times 10^3 \; V_{mm}/(S - S_{ext}) = 2 \times 10^3 \times 0.37/(316 - 8) = 2.4 \text{ nm}$$

using the low-temperature N_2 adsorption/desorption data (Rouquerol *et al.*, 1999). As seen, the average and peak values were approximately the same. Based on this result, the peak radius represents roughly the average micro–mesopore radius.

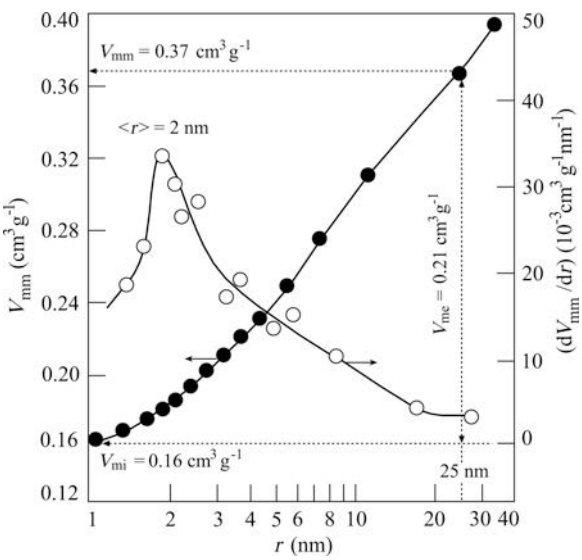

Figure 10. The pore-size distribution curve of V_{mm} *vs.* r and its derivative (dV_{mm}/dr) *vs.* r for the natural sepiolite obtained from the desorption isotherms given in Figure 8 (r: pore radius, V_{mm}: specific micro-mesopore volume, V_{mi}: specific micropore volume, V_{me}: specific mesopore volume).

Potential uses of sepiolites

Sepiolitic clays with different mineralogy and chemical composition have been used for a long time as industrial raw materials in various applications (Robertson, 1957; Chambers, 1959; Preisinger, 1963; Galán, 1996; Murray, 2000). Many of the technological applications are based on the fibrous morphology and nanoporous structure of the mineral (Dandy, 1968; Dandy and Nadiye-Tabbiruku, 1975, 1982; Sarıkaya *et al.*, 1985; Corma and Peréz-Pariente, 1987; Grillet *et al.*, 1988). Sepiolites have also been used recently for the fabrication of all-inorganic ultrafiltration membranes (Weir *et al.*, 2001; Wang *et al.*, 2001).

The significant amount of waste produced by the tobacco-pipe industry and by producers of other souvenirs from Eskişehir sepiolites can be used for several purposes, given the material's large surface area, nanoporosity, and catalytic behavior (Sugahara *et al.*, 1985; Helios-Rybicka, 1985; Ünal and Erdoğan, 1998; Shirvani et. al., 2006). According to previous studies and the present authors' experience, the most important potential uses of the waste from Eskişehir sepiolites are in: ceramics; desiccants; catalyst supports; catalysts; adsorbents of vapors, gases, and heavy metals (from waste water); bleaching earths for vegetable oils; sugar decolorizers; clarifying wine; filter aids; maturation processes in dermatology; deodorants; lubricating-oil refining agents;, paints; greases; inks; pharmaceuticals; cosmetics; *etc*.

CONCLUSIONS

The thermal behavior, crystal structure, and porosity of sepiolite and other pure or mixed minerals were examined using chemical analysis, thermal analysis, particle-size analysis, X-ray diffraction, dilatometry, electron microscopy, mercury porosimetry, and nitrogen adsorption/desorption techniques. The relative amount and the dehydration temperature for the moisture and zeolitic water of the sepiolite cannot be strictly distinguished by thermal analysis. The mechanism for the dehydration of the bound water in the sepiolite requires further study. The sepiolite mineral transforms into sepiolite anhydride, then enstatite, then diopside (with the interference of a calcite impurity) and opal-CT, as the temperature increases from 600 to 1300ºC. After the formation of enstatite, thermal shrinkage appears in the material. A paracrystalline opal-CT forms when the sepiolite is fired at 1200ºC. The XRD peak indicating the formation of opal-CT should not be ascribed to α-cristobalite. Although crystalline α-cristobalite has a similar characteristic d_{101} XRD reflection centered at 0.406 nm, the intensity of the d_{101} XRD reflections for crystalline cristobalite are known not to change when firing from 1200 to 1300ºC, so this peak was assigned to opal-CT. Sepiolite is one of the most porous materials

https://doi.org/10.1346/CCMN.2008.0560504 Published online by Cambridge University Press

among the clay minerals. Its fibrous morphology causes micro-, meso-, and macroporous structures. Macroporosity is greater than the mesoporosity and microporosity together. Good agreement is found between the values of mesoporosity deduced by mercury porosimetry and nitrogen adsorption/desorption. The microporosity calculated from both Dubinin's method using the adsorption data and the bottom limit of the mesopore size-distribution curve obtained from the desorption data was found to be the same. The microporosity measured by the nitrogen adsorption/desorption data does not include the intracrystalline channels in sepiolite. Sepiolites can be used as versatile raw materials in art, science, and technology depending on the physicochemical properties such as mineralogical impurities, chemical composition, thermal behavior, hardness, color, and high porosity.

ACKNOWLEDGMENTS

The authors thank the Scientific and Technical Research Council of Turkey (TÜBİTAK) for supporting this study under project no: TBAG-AY/363 (104T098).

REFERENCES

Akbulut, A. and Kadir, S. (2003) The geology and origin of sepiolite, palygorskite and saponite in Neogene lacustrine sediments of the Serinhisar-Acıpayam basin, Denizli, SW Turkey. *Clays and Clay Minerals*, **51**, 279–292.

Akıncı, Ö. (1967) Eskişehir 124-C_1 paftasının jeolojisi ve tabakalı lületaşı zuhurları. *Maden Tetkik ve Arama Enstitüsü Dergisi (Bulletin of Mining Research and Exploration Institute of Turkey)*, **67**, 82–99.

Aras, A. (2004) The change of phase composition in kaolinite- and illite-rich clay-based ceramic bodies. *Applied Clay Science*, **24**, 257–269.

Arık, H., Kadir, S., and Sarıtaş, S. (1996) Investigation of the structural transformation and refractory properties of the brown sepiolite due to the heating at various temperatures. *Turkish Journal of Engineering and Environmental Sciences*, **20**, 223–244 (in Turkish).

Balcı, S. (1996) Thermal decomposition of sepiolite and variations in pore structure with and without acid pretreatment. *Journal of Chemical Technology and Biotechnology*, **66**, 72–78.

Brunauer, S., Emmett, P.H., and Teller, E. (1938) Adsorption of gases in multimolecular layers. *Journal of the American Chemical Society*, **60**, 308–319.

Campelo, J.M., Garcia, A., Luna, S., and Marinas, J.M. (1987) Catalytic activity of natural sepiolites in cyclohexene skeletal isomerization. *Clay Minerals*, **22**, 233–236.

Çetişli, H. and Gedikbey, T. (1990) Dissolution kinetics of sepiolite from Eskişehir (Turkey) in hydrochloric and nitric acids. *Clay Minerals*, **25**, 207–215.

Chambers, G.P.C. (1959) Some industrial applications of the clay mineral sepiolite. *Silicates Industriels*, 181–189.

Corma, A. and Peréz-Pariente, J. (1987) Catalytic activity of modified silicates: I. Dehydration of ethanol catalyzed by acidic sepiolite. *Clay Minerals*, **22**, 423–433.

Dandy, A.J. (1968) Sorption of vapors by sepiolite. *The Journal of Physical Chemistry*, 334–339.

Dandy, A.J. and Nadiye-Tabbiruku, M.S. (1975) The effect of heating in vacua on the microporosity of sepiolite. *Clays and Clay Minerals*, **23**, 428–430.

Dandy, A.J. and Nadiye-Tabbiruku, M.S. (1982) Surface properties of sepiolite from Amboseli, Tanzania, and its catalytic activity for ethanol decomposition. *Clays and Clay Minerals*, **30**, 347–352.

Dubinin, M.M. (1967) Adsorption in macropores. *Journal of Colloid and Interface Science*, **23**, 487–499.

Ece, Ö.I. and Coban, F. (1994) Geology, occurrence, and genesis of Eskişehir sepiolite, Turkey. *Clays and Clay Minerals*, **42**, 81–92.

Elzea, J.M., Odom, I.E., and Miles, W.J. (1994) Distinguishing well-ordered opal-CT and opal-C from high temperature cristobalite by X-ray diffraction. *Analytica Chimica Acta*, **286**, 107–116.

Esmer, K. (2004) Electrical conductivity and dielectric behavior of modified sepiolite clay. *Applied Clay Science*, **25**, 17–22.

Everett, D.H., Parfitt, G.D., Sing, K.S.W., and Wilson, R. (1974) The SCI/IUPAC/NPL project on surface area standards. *Journal of Applied Chemistry and Biotechnology*, **24**, 199–219.

Galán, E. (1996) Properties and applications of palygorskite-sepiolite clays. *Clay Minerals*, **31**, 443–453.

Galán, E. and Ferrero, A. (1982) Palygorskite-sepiolite clays of Lebrija, southern Spain. *Clays and Clay Minerals*, **30**, 191–199.

Grillet, Y., Cases, J.M., Francois, M., Rouquerol, J., and Poirier, J.E. (1988) Modification of the porous structure and surface area of sepiolite under vacuum thermal treatment. *Clays and Clay Minerals*, **36**, 232–242.

Hang, P.T. and Brindley, G.W. (1970) Methylene blue adsorption by clay minerals. Determination surface areas and cation exchange capacities (Clay-organic studies XVIII). *Clays and Clay Minerals*, **18**, 203–312.

Helios-Rybicka, E. (1985) Sorption of Ni, Zn and Cd on sepiolite. *Clay Minerals*, **20**, 525–527.

Inukai, K., Miyawaki, R., Tomura, S., Shimosaka, K. and İrkoç, T. (1994) Purification of Turkish sepiolites through hydrochloric acid treatment. *Applied Clay Science*, **9**, 11–29.

Kadir, S., Baş, H. and Karakoç, Z. (2002) Origin of sepiolite and loughlinite in a Neogene sedimentary lacustrine environment, Mihalıççık-Eskişehir, Turkey. *The Canadian Mineralogist*, **40**, 1091–1102.

Kahraman, S., Önal, M., Sarıkaya, Y. and Bozdoğan, İ. (2005) Characterization of silica polymorphs in kaolins by X-ray diffraction before and after phosphoric acid digestion and thermal treatment. *Analytica Chimica Acta*, **552**, 201–206.

Karakaya, N., Karakaya, M.Ç., Temel, A., Küpeli, Ş., and Tunaoğlu, C. (2004) Mineralogical and chemical characterization of sepiolite occurrences at Karapınar (Konya Basin, Turkey). *Clays and Clay Minerals*, **52**, 495–509.

Kıyohiro, T. and Otsuka, R. (1989) Dehydration mechanism of bound water in sepiolite. *Thermochimica Acta*, **147**, 127–138.

Kloubek, J. (1981) Hysterisis in porosimetry. *Powder Technology*, **29**, 63–73.

Komarneni, S., Fyte, A., and Kennedy, G.J. (1986) Detection of nonequivalent Si sites in sepiolite and palygorskite by solid-state ^{29}Si magic angle spinning-nuclear magnetic resonance. *Clays and Clay Minerals*, **34**, 99–102.

Kulbicki, C. (1959) High temperature phases in sepiolite attapulgite and saponite. *American Mineralogist*, **41**, 752–758.

Lu, G.Q. and Zhao, X.S. (2004) *Nanoporous Materials.* Series on Chemical Engineering, Vol. 4, Imperial College Press, London.

McKeown, D.A., Post, J.E., and Etz, E.S. (2002) Vibrational analysis of palygorskite and sepiolite. *Clays and Clay Minerals*, **50**, 667–680.

Moore, D.M. and Reynolds, R.C., Jr. (1997) *X-ray Diffraction and the Identification and Analysis of Clay Minerals*, 2nd edition, Oxford University Press, New York.

Moscou, L. and Lub, S. (1981) Practical use of mercury porosimetry in the study of porous solids. *Powder Technology*, **29**, 45–52.

Murray, H.H. (2000) Traditional and new applications for kaolin, smectite and palygorskite. A general overview. *Applied Clay Science*, **17**, 207–221.

Önal, M., Kahraman, S., and Sarıkaya, Y. (2007) Differentiation of α-cristobalite from opals in bentonites from Turkey. *Applied Clay Science*, **35**, 25–30.

Özdemir, M. and Kıpçak, İ. (2004) Dissolution kinetics of sepiolite in hydrochloric acid nitric acid. *Clays and Clay Minerals*, **52**, 714–720.

Otsuka, R., Mariko, T., and Sakamoto, T. (1973) Mineralogische eigenschaften vom Meerschaum von Eskişehir, Türkei. *Memoirs of the School of Science and Engineering*, **37**, 43–52.

Post, J.L. (1978) Sepiolite deposits of the Las Vegas, Nevada area. *Clays and Clay Minerals*, **26**, 58–64.

Preisinger, A. (1959) X-ray study of the structure of sepiolite. *Clays and Clay Minerals*, **6**, 61–67.

Preisinger, A. (1963) Sepiolite and related compounds: its stability and applications. *Clays and Clay Minerals*, **10**, 365–371.

Rautureau, M. and Yücel, A. (1976) Etude par microscopie et microdiffraction electronique de l'ecume de mer, pole mal Cristallise de la famille des sepiolites. *Journal de Microscopie et de Spectroscopie Électronique*, **1**, 405–414.

Robertson, R.H.S. (1957) Sepiolite: a versatile raw material. *Chemistry and Industry*, 1492–1495.

Rouquerol, F., Rouquerol, J., and Sing, K. (1999) *Adsorption by Powders and Porous Solids*. Academic Press, London.

Rytwo, G., Serben, C., Nir, S., and Margulies, L. (1991) Use of methylene blue and crystal violet for determination of exchangeable cations in montmorillonite. *Clays and Clay Minerals*, **39**, 551–555.

Sarıkaya, Y. and Aybar, S. (1978) The adsorption of NH_3, N_2O and CO_2 gases on the 5A molecular sieve. *Communications (Faculty of Science, University of Ankara)*, **B24**, 33–39.

Sarıkaya, Y., Yücel, A., Eğilmez, Ö., Makul, G., Almac, R., Harman, I., and Bozdoğan, İ. (1985) Evaluation of sepiolite wastes: use in cigarette filters. *Doğa Bilim Dergisi*, **B9**, 277–287 (in Turkish).

Sarıkaya, Y., Önal, M., Baran, B., and Alemdaroğlu, T. (2000) The effect of thermal treatment on some of the physico-chemical properties of a bentonite. *Clays and Clay Minerals*, **48**, 557–562.

Serna, C., Ahlrichs, J.L., and Serratosa, J.M. (1975) Folding in sepiolite crystals. *Clays and Clay Minerals*, **23**, 452–457.

Shirvani, M., Kalbasi, M., Shariatamadari, Nourbaksh, F., and Najati, B. (2006) Sorption-desorption of cadmium in aqueous palygorskite, sepiolite and calcite suspensions: Isotherm hysteresis. *Chemosphere*, **65**, 2178–2184.

Sugahara, Y., Kurada, K., and Kato, C. (1985) Nitridation of sepiolite by carbothermal reduction. *Journal of Materials Science Letters*, **4**, 928–931.

Sugiura, M., Hayashi, H., and Suzuki, T. (1991) Adsorption of ammonia by sepiolite in ambient air. *Clay Science*, **8**, 87–100.

Ünal, H.I. and Erdoğan, B. (1998) The use of sepiolite for decolorization of sugar juice. *Applied Clay Science*, **12**, 419–429.

Wang, Q.K., Matsuura, T., Feng, C.Y., Weir, M.R., Detellier, C., Rutinduka, E., and Le Van Mao, R. (2001) The sepiolite membrane for ultrafiltration. *Journal of Membrane Science*, **184**, 153–163.

Weir, M.R., Rutinduka, E., Detellier, C., Feng, C.Y., Wang, Q.K., Matsura, T., and Le Van Mao, R. (2001) Fabrication ultrafiltration membranes composed entirely of a naturally occurring sepiolite clay mineral. *Journal of Membrane Science*, **182**, 41–50.

Weir, M.R., Kuang, W.K., Facey, G.A., and Detellier, C. (2002) Solid-state nuclear magnetic resonance study of sepiolite and partially dehydrated sepiolite. *Clays and Clay Minerals*, **50**, 240–247.

Yalçın, H. and Bozkaya, Ö. (1995) Sepiolite-palygorskite from the Hekimhan region (Turkey). *Clays and Clay Minerals*, **43**, 705–717.

Yalçın, H. and Bozkaya, Ö. (2004) Ultramafic-rock-hosted vein sepiolite occurrences in the Ankara ophiolitic melange, central Anatolia, Turkey. *Clays and Clay Minerals*, **52**, 227–239.

Yücel, A., Rautureau, M., Tchoubar, D., and Tchoubar, C. (1980) Calculation of the X-ray powder reflection profiles of very small needle-like crystals. I. Principles of the method. *Journal of Applied Crystallography*, **13**, 370–374.

(*Received 8 May 2007; revised 2 July 2008; Ms. 0028; A.E. J. Amonette*)